Are Sieving and Sedimentation Still Fit-for-Purpose? A Comparison with Dynamic Image Analysis for Soil PSD

Gianmario Sorrentino[a,*], Mauro Muñiz-Menéndez[b] and Pieter Desnerck[a,*]

[a]Department of Engineering, University of Cambridge, 7a JJ Thomson Ave Cambridge CB3 0FA, UK
[b]CEDEX. Laboratorio de Geotecnia, Madrid, Spain

ARTICLE INFO

Keywords:
Soil characterization
Particle size distribution
Dynamic image analysis
Sedimentation
Particle morphology

ABSTRACT

Particle size distribution (PSD) is a fundamental parameter in soil characterization because it strongly influences macroscopic properties such as packing, pore structure, permeability, and mechanical behaviour. In routine geotechnical practice, PSD is still mainly determined by dry sieving for coarse fractions and sedimentation for fines. Although these methods are standardized and widely used, they provide method-defined size measures and do not capture particle morphology. Dynamic image analysis (DIA) offers an alternative by measuring both particle size and shape with lower operator burden and potentially lower cost.

This study evaluates whether conventional PSD methods remain fit for purpose by comparing dry sieving and sedimentation with DIA across shape-controlled reference materials and representative engineering soils and powders. For coarse particles, the DIA minimum-dimension metric showed the closest agreement with sieving, confirming that sieve-based sizing is primarily controlled by the smallest particle dimension. For fine materials, sedimentation generally agreed best with minimum-type DIA metrics, but agreement decreased toward the finest sizes and deteriorated markedly for clay-rich materials. Overall, conventional methods remain useful reference procedures, whereas DIA provides a faster and more informative route to PSD determination, supporting more reliable method selection in laboratory practice.

1. Introduction

Particle size distribution (PSD) is a first-order descriptor of granular material. It controls packing, pore-size structure, permeability and mechanical response (Bareither et al., 2008; Li and Iskander, 2020; Mitchell and Soga, 2005; Zheng and Hryciw, 2016). It also influences transport and surface-controlled processes (e.g., sedimentation, dissolution, and adsorption) (Ranville and Montano, 2015; Weiss et al., 2013). Particle shape adds an additional layer of control: elongation, angularity, and surface texture affect interlocking and fabric development, while departures from sphericity alter settling behaviour and optical responses (Cho et al., 2006; Sedláčková et al., 2024; Wang et al., 2019). As a result, materials with similar median size can behave very differently if their particle morphologies differ, and any sizing method that implicitly assumes spherical particles can introduce systematic bias when applied to platy, elongated, or highly irregular grains.

Traditional PSD methods—dry sieving for coarse fractions and sedimentation-based methods (hydrometer or pipette) for fines—remain the backbone of routine soil classification and are embedded in standards and long-term datasets. Their continued use is motivated by familiarity, standardisation, and comparability with historical practice. However, both methods are fundamentally operational. Sieving classifies particles by their ability to pass through an aperture under agitation, which depends on particle orientation and a controlling dimension. Sedimentation infers an equivalent spherical diameter from settling behaviour and therefore relies on assumptions that can be violated by non-spherical particles, aggregation/flocculation, or departures from the Stokes regime.

Instrument-based techniques are also becoming increasingly accessible in routine laboratory practice. In particular, dynamic image analysis (DIA) provides rapid measurements on large particle populations and reports both PSDs and particle morphology descriptors (e.g., aspect ratio, sphericity, convexity, and roundness) from 2D particle projections (Pons and Dodds, 2015; Rabinski and Thomas, 2004). At the same time, DIA results remain definition-dependent: the

*Corresponding authors
gs581@cantab.ac.uk (G. Sorrentino); Mauro.Muniz@cedex.es (M. Muñiz-Menéndez); prhd2@cam.ac.uk (P. Desnerck)
ORCID(s): 0000-0002-9890-6032 (G. Sorrentino); 0000-0001-5202-0044 (M. Muñiz-Menéndez); 0000-0002-8042-9741 (P. Desnerck)

reported PSD changes with the selected equivalent diameter (area-, perimeter-, Feret- or circle-based), and outcomes can be influenced by particle orientation and image processing choices.

Consequently, disagreements between *traditional* and *modern* techniques may reflect differences in measurement principle and size definition, rather than experimental error alone. As modern sizing technologies become increasingly accessible, the key issue is no longer simply whether methods agree, but whether conventional methods remain fit for purpose for routine PSD determination, given the labour, turnaround time, and operational burden required to perform them reliably.

Several studies have compared conventional and image-based particle-sizing methods, but these comparisons have generally focused on specific materials or application-driven problems rather than on a broader assessment of routine PSD determination across soil-relevant particle types (Al-Hashemi et al., 2021; Callesen et al., 2023; Lopez et al., 2021; Ryzak and Bieganowski, 2010). Addressing this gap requires not only comparing methods, but also clarifying *why* they differ, particularly with respect to particle shape and the choice of equivalent diameter in DIA.

This study aims to move the discussion from *old versus new* to *fitness-for-purpose*. Conventional methods (dry sieving and sedimentation) are compared with DIA across both coarse and fine materials using a two-stage material selection. First, manufactured reference particles with controlled and reproducible geometries were used, including coarse pasta shapes and fine shape end-members such as glass spheres and cellulose, so that differences could be interpreted primarily in terms of measurement principle and size definition. Second, the comparison was extended to materials commonly encountered in research and engineering practice, namely quartz sands and fine industrial minerals/clays, where natural variability and fines behaviour can amplify method-dependent discrepancies.

To emphasise practical relevance, the conventional tests were performed following standard laboratory procedures rather than as idealised research demonstrations. Sedimentation testing was carried out at CEDEX (Madrid, Spain) according to ISO 17892-4:2016, while sieving was performed at NRFIS (Cambridge, UK) using the sieve series defined in BS EN 933-2:2020; where appropriate, supplier-provided grading information was also used for sand products. This experimental design reflects how PSD data are generated in practice and allows the results to be interpreted in the context of routine laboratory workflows.

By combining controlled reference particles with engineering materials across both fine and coarse size ranges, this study provides a broader framework for interpreting agreement and disagreement between conventional PSD methods and DIA. In doing so, it clarifies the practical limits of each method and supports more informed selection of PSD techniques for different materials and applications.

1.1. Background: conventional and image-based PSD methods

1.1.1. Dry sieving

Sieving is one of the oldest methods for particle-size classification, with origins in early grain separation and mineral processing. A major step toward modern analytical practice came with von Rittinger's 1867 proposal of test sieves arranged in a geometric series of openings (Allen, 1990), a concept later formalised in standards such as ASTM E11 and ISO 565:1990, which define sieve dimensions and aperture series to ensure reproducible particle-size analysis across laboratories.

In dry sieving, particles are separated according to their ability to pass through mesh openings under agitation (Barnes, 2017; Germaine and Germaine, 2009). The resulting size classes are therefore operational measures rather than direct geometric diameters, because passage depends on particle orientation and shape. For non-spherical grains—especially elongated or flaky ones—the measured sieve size is typically governed by a controlling projection (often closer to the intermediate or minimum dimension) rather than the maximum dimension (Bartley III et al., 2019; Fernlund, 1998), as shown in Fig. 1.

Because granular materials often span wide size ranges, sieve apertures are commonly arranged in a geometric progression, and PSDs are typically plotted on a logarithmic diameter axis. This convention improves readability across fine and coarse fractions and is consistent with the frequently observed log-normal character of many natural granular systems (ASTM, 2009).

Practical limitations of dry sieving include sieve blinding, sensitivity to shaking conditions (Bartley III et al., 2019), and a lower practical size limit, typically taken as 75 µm under ASTM D6913-04 and 63 µm under ISO 17892-4:2016, below which cohesive forces and agglomeration compromise separation. Despite these constraints, dry sieving remains a robust and widely standardised method for grading non-cohesive particulate materials.

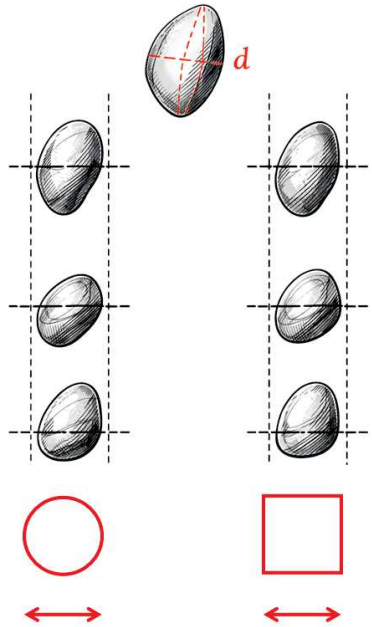

Figure 1: Schematic illustration of orientation effects in sieving. Adapted from Urciuoli (2007).

1.1.2. Sedimentation-based PSD

For fine-grained soils (particle sizes smaller than 75 µm), particle size distributions are commonly determined by sedimentation methods (e.g., hydrometer or pipette tests) as specified in geotechnical standards such as ISO 17892-4:2016. These methods infer an equivalent particle diameter from the settling behaviour of particles in a fluid, providing a practical extension of PSD determination into the silt and clay size range where sieving becomes unreliable (ASTM D1140).

Sedimentation-based sizing is typically interpreted using Stokes' law for spheres, which relates terminal settling velocity to the square of particle diameter under low Reynolds number conditions. It should be noted that sizes inferred from Stokes-type settling relations do not represent true particle diameters, but rather *equivalent spherical diameters* that would settle at the same velocity under the assumed conditions. In practice, gravity sedimentation is applicable over a limited size range, commonly cited as approximately 200 µm to 0.2 µm: the upper bound reflects the transition away from laminar (Stokes) flow around the particle, while the lower bound reflects the increasing importance of Brownian motion, which can keep the finest particles in suspension for very long times (Mitchell and Soga, 2005).

For non-spherical particles, the mapping between settling velocity and an equivalent diameter is not unique because hydrodynamic drag depends on particle shape and, for anisotropic particles, on orientation. Classical work on particle motion in viscous flow (Jeffery, 1922) and subsequent developments in drag correlations (Michaelides, 2026) highlight that elongated particles can experience orientation-dependent resistance. Experimental observations further show that freely falling cylinders and cones adopt preferred orientations during settling, and that their terminal velocity and drag depend on the fall attitude (Jayaweera and Mason, 1965). Consequently, if sedimentation data are interpreted using a spherical assumption, elongated or platy particles may yield biased size estimates because their effective drag differs from that of a sphere and may vary with the preferred settling orientation.

1.1.3. Dynamic image analysis (DIA)

Digital image analysis (DIA) emerged as a non-contact approach to particle characterisation as imaging systems and computer processing became sufficiently fast and accurate to extract size and shape information directly from particle images (Pons and Dodds, 2015; Rabinski and Thomas, 2004). It developed from earlier optical microscopy and image-processing approaches, but with substantially higher throughput, enabling statistically robust measurements based on large particle counts. A key advantage of DIA is that it quantifies not only particle size but also particle morphology through descriptors extracted from 2D projections.

Historically, particle shape assessment was often based on visual interpretation of particle images. In sedimentology, for example, roundness was commonly estimated using reference charts, notably those proposed by Krumbein and Sloss (1963) and later refined by Powers (1953). DIA can be viewed as a quantitative extension of these image-based approaches, replacing visual classification with automated extraction of geometric descriptors from digital images.

In a typical DIA measurement, particles are dispersed into a controlled stream (or free-fall curtain, depending on the particle size range) so that they pass the imaging window individually and with minimal overlap. High-resolution images are acquired and converted into binary particle silhouettes, from which the software computes equivalent diameters (e.g., area- or perimeter-equivalent, Feret-based, or inscribed/circumscribed-circle measures) together with shape descriptors. Fig. 2 provides a schematic overview of the DIA workflow adopted in this study. Because DIA is based on 2D projections, the reported size remains definition-dependent and can be influenced by particle orientation and the imaging/segmentation protocol; nevertheless, it provides a practical and information-rich alternative to traditional PSD methods, particularly for irregular and non-spherical particles.

Other instrument-based methods, such as laser diffraction, are also widely used for particle-size analysis (Eshel et al., 2004), particularly for fine materials (Bittelli et al., 2022); however, they were not considered here because the focus of this study was on comparing conventional geotechnical methods with dynamic image analysis, which additionally provides particle morphology information.

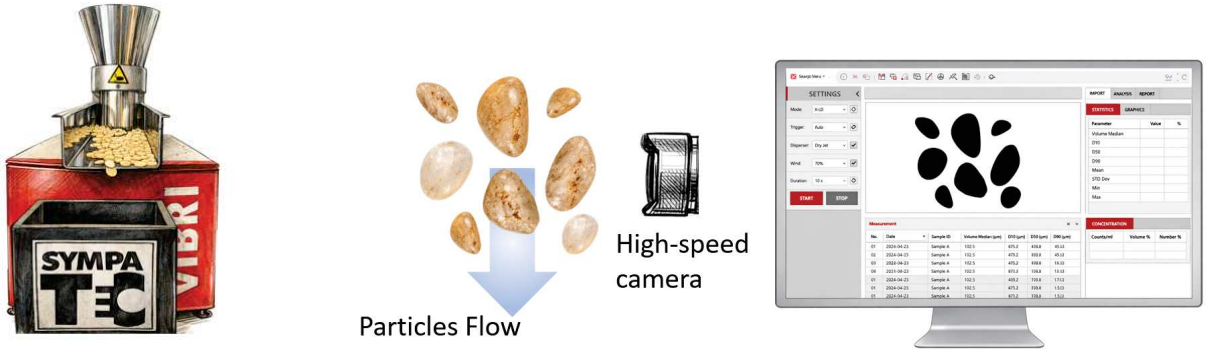

(a) (b) (c)

Figure 2: Schematic overview of the dynamic image analysis (DIA) workflow: (a) particles are dispersed into a controlled stream so that they pass the imaging window individually with minimal overlap; (b) a high-resolution camera records particle images, which are converted to binary silhouettes; (c) the instrument software then computes equivalent diameters and shape descriptors from the 2D projections.

2. Materials and Methods

2.1. Material

To compare traditional particle sizing methods (sieving and hydrometer) with dynamic image analysis techniques (Sympatec QicPic and the Anton Paar Litesizer DIA), we selected two complementary groups of materials. First, manufactured reference materials with well-defined particle geometries were used, including pasta for coarse particles and glass spheres and cellulose for fines. These materials were selected to approximate an idealised case in which particles within a sample are intentionally uniform and their geometry is known, allowing differences between traditional PSD methods and dynamic image analysis to be attributed primarily to the measurement principle and the definition of the reported size metric. This set was chosen to explicitly investigate how particle shape influences the PSD and shape metrics reported by different techniques under controlled conditions. Second, to place the findings in a practical context, the comparison was extended to real granular and fine-grained materials commonly used in research and engineering applications. These materials introduce natural variability in surface properties and shape, allowing the observations from the reference particles to be evaluated under conditions representative of engineering material characterization across geotechnical and construction-related applications, including the characterization of concrete constituents.

Table 1
Morphological descriptors of the different materials.

	Sphericity		Aspect Ratio		Convexity		Roundness	
Material	**Mean ± Std**	**CV**	**Mean ± Std**	**CV**	**Mean ± Std**	**CV**	**Mean ± Std**	**CV**
Barite	0.948 ± 0.043	0.05	0.733 ± 0.118	0.16	0.973 ± 0.025	0.03	0.720 ± 0.121	0.17
Cellulose	0.801 ± 0.115	0.14	0.485 ± 0.192	0.40	0.909 ± 0.072	0.08	0.444 ± 0.184	0.41
Glass sphere	0.966 ± 0.098	0.10	0.880 ± 0.136	0.15	0.971 ± 0.072	0.07	0.880 ± 0.151	0.17
$CaCO_3$ F8	0.940 ± 0.050	0.05	0.706 ± 0.125	0.18	0.972 ± 0.030	0.03	0.691 ± 0.127	0.18
$CaCO_3$ F22	0.921 ± 0.059	0.06	0.674 ± 0.129	0.19	0.965 ± 0.036	0.04	0.646 ± 0.129	0.20
$CaCO_3$ F150	0.932 ± 0.048	0.05	0.717 ± 0.122	0.17	0.969 ± 0.028	0.03	0.681 ± 0.118	0.17
Bentonite	0.937 ± 0.047	0.05	0.710 ± 0.128	0.18	0.970 ± 0.025	0.03	0.687 ± 0.131	0.19
Kaolinite	0.931 ± 0.065	0.07	0.693 ± 0.139	0.20	0.965 ± 0.041	0.04	0.680 ± 0.146	0.21

2.1.1. Fine Material

For the fine fraction, glass spheres and microcrystalline cellulose powder (cellulose) particles were selected as shape-controlled reference materials, representing near-spherical and elongated/fibrous morphologies (Falahati et al., 2020; Sorrentino, 2022). To extend the fine dataset across a broader size range, calcium carbonate ($CaCO_3$) powders with specified nominal diameters were also tested. In particular, the $CaCO_3$ grade F150 was included to ensure coverage of the sedimentation-controlled domain, since hydrometer/sedimentation methods are typically applied for particle sizes smaller than 75 µm. In addition to the reference materials, fine-grained powders commonly used in laboratory research and engineering practice were tested. These included barite and bentonite, both widely employed as weighting and viscosifying/filtration-control additives in drilling-fluid formulations (Sorrentino and Biscontin, 2023; Sorrentino et al., 2025), and kaolinite, which is frequently used as a reference clay in geotechnical and soil science studies (Kenney, 1967; Nasser and James, 2006). The morphological descriptors obtained from DIA measurements for the fine materials are summarised in Tab. 1.

Fig. 3a illustrates the range of fine-particle morphologies considered in this study. In the sphericity versus aspect ratio plane, glass spheres and cellulose occupy the two extremes: the spheres form the near-spherical end-member (high sphericity and high aspect ratio), whereas cellulose represents the elongated/fibrous end-member (low aspect ratio and lower sphericity). The remaining fine powders cluster between these bounds, generally closer to the spherical end-member, indicating a broad but realistic morphology range with well-defined extremes.

The corresponding size coverage is summarised in Fig. 3b. Most fine materials span median sizes of approximately 5 µm to 50 µm, while $CaCO_3$ F150 extends the dataset to the coarser end of the fine fraction, linking the DIA comparison to the transition towards sieve-controlled sizing.

2.1.2. Coarse Material

For coarse particles with controlled and contrasting geometries, three pasta types were selected-*risoni*, *puntine*, and *tempestine*-as shown in Fig. 4. The set spans a wide morphology range: risoni and puntine are markedly elongated, whereas tempestine is more compact, approximating a short cylinder. Because these manufactured materials have controlled and repeatable geometries, they provide a benchmark dataset in which particle morphology is known *a priori*. This makes it possible to assess how particle shape influences the PSD reported by sieving and by DIA, without confounding effects from the broader heterogeneity typically present in natural sands.

As representative natural granular materials, Danish sand (DanSand) (Otim et al., 2025; Sorrentino and Franza, 2025), Leighton Buzzard sand (Cavallaro et al., 2001; Penna et al., 2016; Senetakis et al., 2013), and a *sharp sand* supplied by Cardinalis, commonly used in building materials and concrete (Forsdyke and Lees, 2025), were tested. Danish sand and Leighton Buzzard sand (LBS) were analysed as sieve fractions and thus represented relatively uniform sands (e.g. $U \approx 1.3$ for LBS, and $U \approx 2.0$ for DanSand), whereas the sharp sand was included as a contrasting non-uniform material ($U \approx 3.6$). The *sharp sand* was composed of two distinct fractions: a finer fraction centred around

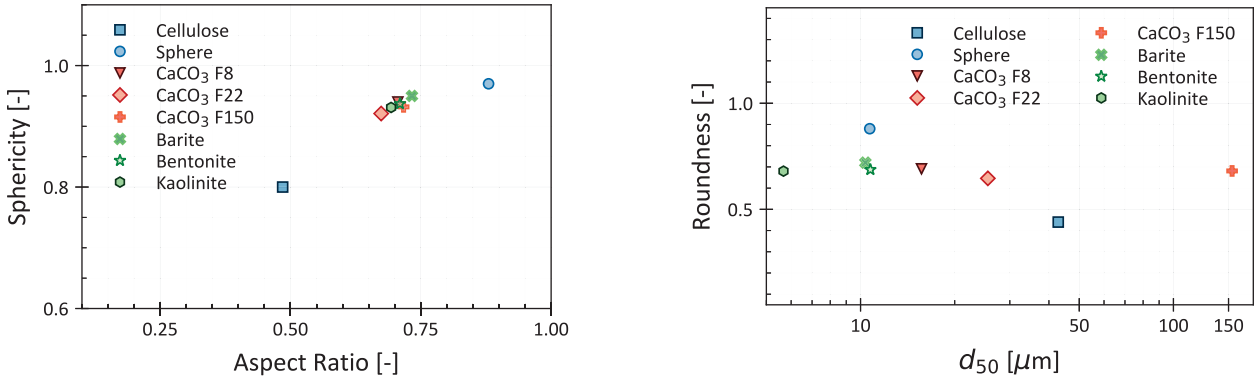

Figure 3: Summary of the morphology of the fine materials analysed: (a) Sphericity versus aspect ratio; (b) Roundness versus median size (d_{50}).

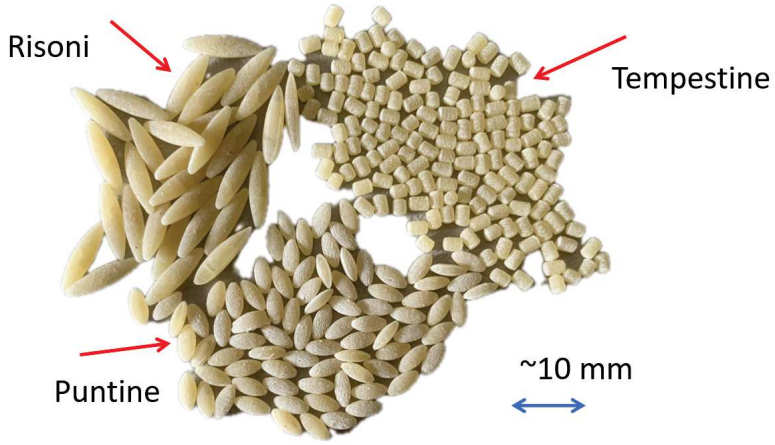

Figure 4: Coarse manufactured reference particles used in this study, showing the three pasta types selected as shape-controlled materials: *risoni*, *puntine*, and *tempestine*.

0.4 mm and a coarser fraction centred around 4 mm; the overall distribution was characterised by $D_{50} \approx 0.65$ mm and $D_{90} \approx 4.20$ mm, as shown in Fig. 5.

Tab. 2 summarises the morphological descriptors of the coarse materials tested, while Fig. 6 provides a visual representation of their distribution in the sphericity-aspect ratio plane. For *sharp sand*, which was not fractionated and had a broad bimodal grading, the reported descriptors are volume-weighted averages from the DIA data. The pasta particles span a broad range of aspect ratios (approximately AR 0.30 to 0.75), whereas the sand fractions cluster within a comparatively narrow band of aspect ratio and sphericity, indicating more limited variability in these descriptors for the natural sands.

2.2. Conventional PSD methods (sieving and sedimentation)

Conventional particle size distributions were obtained using dry sieving for the coarse materials and sedimentation (hydrometer) testing for the fine fraction. Where available, supplier-provided grading information was used for natural sands.

2.2.1. Dry sieving

Dry sieving of the pasta samples was carried out at NRFIS using a stack of test sieves with nominal aperture sizes of 4.75 mm, 4.0 mm, 3.35 mm, 2.0 mm, 1.18 mm, 1.0 mm, 0.85 mm, 0.6 mm and 0.3 mm. These aperture sizes are

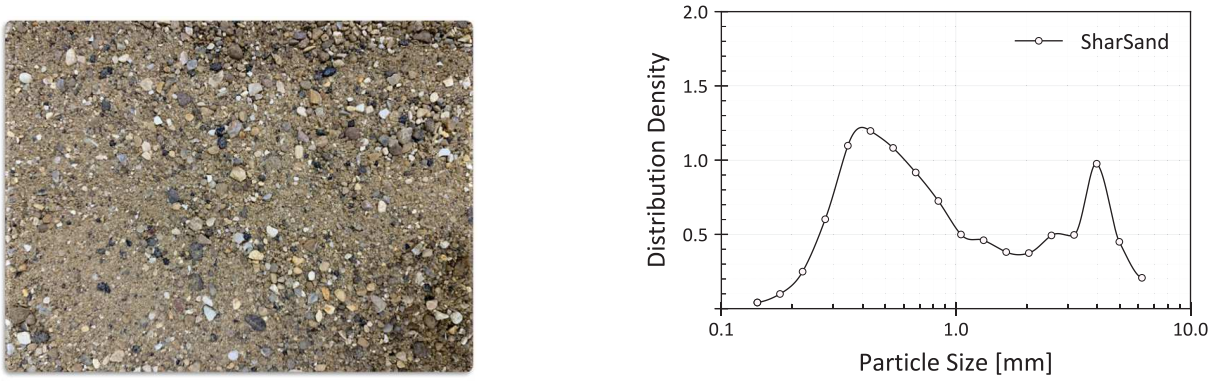

(a) (b)

Figure 5: *Sharp sand* used in this study: (a) photograph of the material; (b) Volume distribution density particle size distribution.

Table 2
Morphological descriptors of the different samples.

	Sphericity		Aspect Ratio		Convexity		Roundness	
Material	**Mean**	**CV**	**Mean**	**CV**	**Mean**	**CV**	**Mean**	**CV**
Risoni	0.71 ± 0.08	0.11	0.32 ± 0.12	0.38	0.98 ± 0.01	0.01	0.16 ± 0.09	0.58
Tempestine	0.81 ± 0.04	0.05	0.73 ± 0.07	0.09	0.99 ± 0.00	0.00	0.13 ± 0.05	0.42
Puntine	0.82 ± 0.05	0.06	0.50 ± 0.10	0.21	0.98 ± 0.01	0.01	0.24 ± 0.11	0.4
LBS-Fraction A	0.84 ± 0.05	0.06	0.72 ± 0.11	0.16	0.96 ± 0.02	0.02	0.33 ± 0.13	0.38
LBS-Fraction B	0.83 ± 0.05	0.06	0.70 ± 0.13	0.18	0.95 ± 0.03	0.03	0.35 ± 0.19	0.56
LBS-Fraction C	0.83 ± 0.04	0.05	0.72 ± 0.11	0.15	0.97 ± 0.02	0.02	0.26 ± 0.09	0.36
LBS-Fraction D	0.82 ± 0.04	0.05	0.72 ± 0.11	0.15	0.96 ± 0.02	0.02	0.34 ± 0.09	0.26
LBS-Fraction E	0.82 ± 0.07	0.08	0.74 ± 0.12	0.16	0.94 ± 0.03	0.03	0.39 ± 0.14	0.37
DanSand	0.84 ± 0.05	0.06	0.72 ± 0.12	0.17	0.94 ± 0.03	0.03	0.41 ± 0.23	0.57
Sharp sand*	0.88 ± 0.04	0.04	0.72 ± 0.11	0.15	0.95 ± 0.02	0.03	0.41 ± 0.38	0.88

*Morphological descriptors are reported as number-based averages from the DIA data. For *sharp sand* the reported descriptors were calculated as volume-weighted averages from the DIA data.

consistent with commonly used nominal sieve series (e.g., ASTM D6913-04). The mass retained on each sieve was recorded and converted to cumulative passing to obtain the sieve-based PSD.

For the natural sands, grading information was taken from supplier documentation. For Danish sand, the supplier-provided sieve analysis was used. For Leighton Buzzard sand, the supplied fractions (and their corresponding size bounds) were used to define the coarse size classes considered in this study.

2.2.2. Sedimentation (hydrometer) testing

Sedimentation (hydrometer) tests were carried out at CEDEX (Centro de Estudios y Experimentación de Obras Públicas), Madrid, Spain, following ISO 17892-4:2016 for specimen preparation, dispersion, and temperature control. Preliminary tests showed that the glass-bead material did not provide a reliable sedimentation response under the standard configuration, likely due to density-related limitations of the test fluid. Alternative fluids and configurations

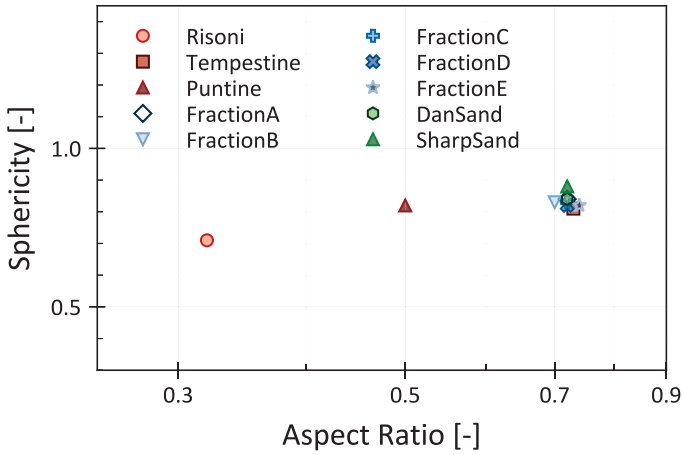

Figure 6: Sphericity versus aspect ratio for the coarse materials analysed.

were considered, but a full investigation was beyond the scope of this work; consequently, reliable sedimentation-based particle size results could not be obtained for this material.

2.3. Dynamic image analysis (DIA)

Dynamic image analysis was carried out using two instruments: the QicPic at NRFIS, Cambridge, for coarse materials, and the Anton Paar Litesizer at CEDEX, Madrid, for fine materials. Both systems determine particle size and shape from 2D particle projections (silhouettes) recorded during measurement. The DIA measurements were evaluated in accordance with ISO 13320:2020, which was preferred over ISO 13322-2:2021 for practical reasons. As discussed by Li and Iskander (2020), the procedure in ISO 13322-2:2021 requires estimating the number of imaged particles needed to achieve a target accuracy, which is difficult in practice because this number cannot be known a priori and DIA captures only a subset of the particles in the specimen. Particle *size* is reported through one or more *equivalent diameters* derived from the 2D particle projection. The main size definitions used in this study include area-equivalent, perimeter-equivalent, Feret-based, and inscribed/circumscribed-circle measures, each representing a different geometric aspect of the projected particle. Particle *shape* is quantified from the same projection using dimensionless descriptors such as aspect ratio (AR), sphericity (S), convexity (C_v), and roundness (R). A schematic overview of the main size and shape definitions used in this work is provided in Fig. 7.

2.3.1. QicPic

Measurements for the coarse material were performed using a QicPic dynamic image analyser. The instrument provides both (i) particle-level data (individual particle size and shape descriptors) and (ii) aggregated particle size distributions (PSDs). In this study, QicPic results were evaluated using multiple size indices, including area-equivalent and perimeter-equivalent diameters, as well as circle-based metrics (e.g., maximum inscribed circle and minimum circumscribed circle). Shape descriptors were obtained directly from the QicPic software outputs for each particle and subsequently summarised at the sample level.

QicPic measurements require the operator to define the dispersion and feeding conditions (e.g., vibration intensity, feed rate/conveyor speed, and drop height) to obtain a stable particle stream and minimise particle overlap in the recorded images. For each material, several preliminary runs were performed to adjust these settings. The final settings were selected once repeated measurements were consistent and visual inspection of the recorded frames indicated negligible particle superposition. For each test, a small mass of material (approximately one teaspoon, 5 g to 15 g) was sufficient. The analysed particle count was typically on the order of 1×10^3 particles for the pasta samples and 3×10^3 to 5×10^3 particles for the sand fractions.

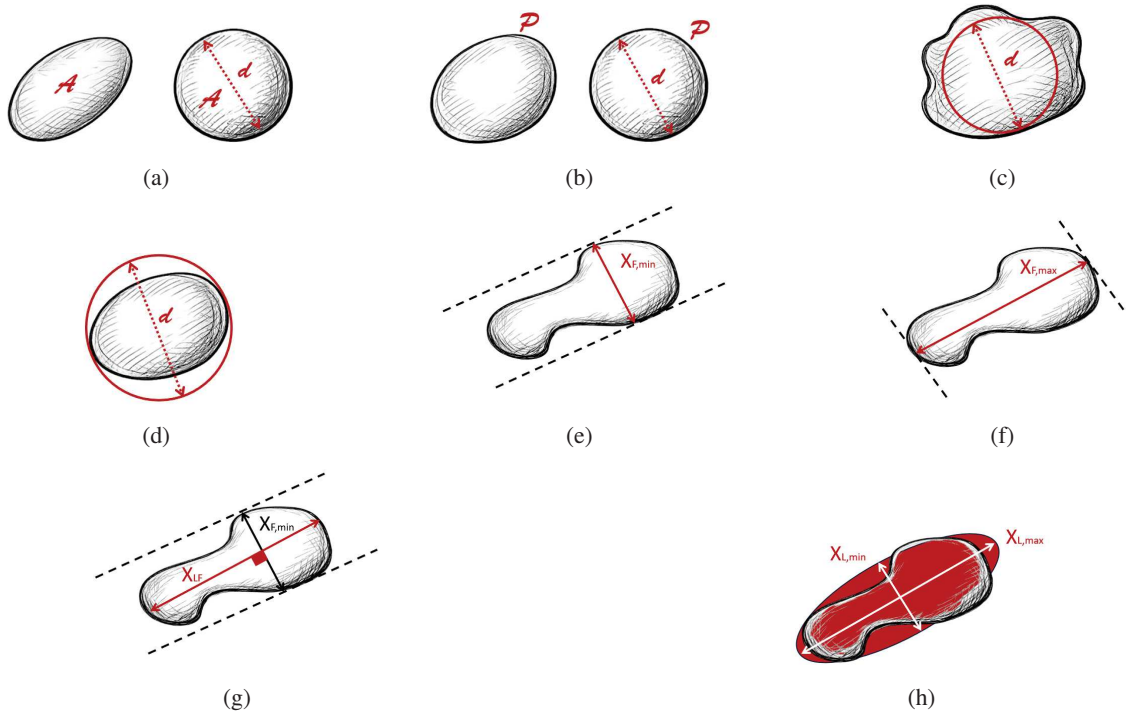

Figure 7: Schematic illustration of the QicPic size indices used in this study: (a) area-equivalent diameter (EQPC); (b) perimeter-equivalent diameter (PED); (c) maximum inscribed circle (MIC); (d) minimum circumscribed circle (MCC); (e) minimum Feret diameter ($x_{F,\min}$); (f) maximum Feret diameter ($x_{F,\max}$); (g) length of the fibre/length-based measure (x_{LF}); and (h) minimum and maximum length-based diameters ($x_{L,\min}$ and $x_{L,\max}$). Partly adapted from Anton Paar Wiki, "Dynamic Image Analysis: Principles, Data Quality, and Applications".

2.3.2. Litesizer DIA

Measurements for the fine material were performed using the Anton Paar Litesizer DIA. In contrast to QicPic, the Litesizer DIA provides PSD outputs for the selected size definition(s), but does not export the full particle-by-particle dataset required for additional custom post-processing.

As for QicPic, the measurement requires the operator to define dispersion and feeding conditions (e.g., flow/feed rate and related instrument settings) to obtain a stable particle stream and minimise particle overlap. Several preliminary runs were conducted to adjust these parameters; the final settings were selected once repeat measurements were consistent. For each material, replicate measurements were then performed, typically analysing on the order of 1×10^4 to 1×10^5 particles per sample.

3. Results and Discussion

3.1. Sedimentation versus dynamic image analysis (QicPic)

Fig. 8 compares PSDs obtained by sedimentation and by DIA for the shape-controlled reference materials: cellulose (Fig. 8a) and glass sphere (Fig. 8b). For cellulose, the sedimentation PSD falls within the envelope of DIA PSDs obtained using the different DIA size definitions, and it was closest to the minimum-dimension metrics (e.g., $x_{F,\min}$ and $x_{L,\min}$). This is consistent with the strongly elongated shape of the cellulose particles.

The reason is that sedimentation does not measure a geometric particle size directly; it reports the diameter of a sphere that would settle at the same velocity. For elongated particles, this equivalent diameter is controlled mainly by hydrodynamic drag and therefore depends on both particle shape and settling orientation (Yokojima et al., 2021). In the Stokes regime, symmetric non-spherical particles may retain their initial orientation during settling (McNown and Malaika, 1950). At higher Reynolds numbers, however, they can rotate towards a stable orientation, which has been reported to correspond to the maximum principal cross-sectional area normal to the settling direction (McNown and

Malaika, 1950; Sheikh et al., 2020). For elongated particles, this broadside orientation increases drag, slows settling, and leads to a smaller sedimentation-equivalent diameter. As a result, the sedimentation size tends to shift away from the particle length and towards values closer to the minor dimension. For cellulose, this explains why the sedimentation PSD was closest to the minimum-type DIA sizes and appeared comparatively narrow.

The uniformity coefficients support this interpretation. For cellulose, DIA gives U values in the range 2.35 to 3.35, depending on the selected size definition, whereas sedimentation gives $U = 1.83$. Sedimentation, therefore, gave a narrower apparent PSD. This does not necessarily mean that the cellulose was more uniform. Rather, sedimentation reduces particle shape to a single hydrodynamic equivalent size, and elongated particles may also settle in similar orientations. DIA was more sensitive to particle geometry because it measured projected dimensions from images, which vary with particle pose and with the selected size definition. As a result, DIA shows a broader distribution for the same material.

A further observation from Fig. 8 is that the spread between DIA PSDs computed using minimum- and maximum-type size definitions (e.g., $x_{L,\mathrm{min}}$ versus $x_{L,\mathrm{max}}$) was substantially larger for cellulose than for the spheres. Although DIA directly reports shape descriptors, this result illustrates that the *dispersion* between PSDs derived from different DIA size definitions can itself indicate particle anisotropy: highly elongated particles exhibit a larger separation between minimum- and maximum-based equivalent diameters than more equant particles.

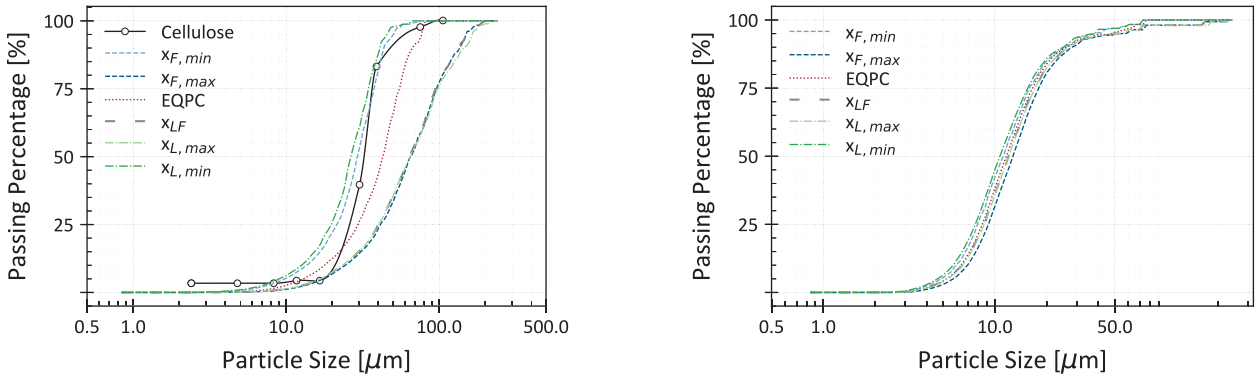

Figure 8: Comparison between PSDs obtained by sedimentation and by dynamic image analysis (DIA) for shape-controlled reference materials: (a) cellulose; (b) glass spheres.

Fig. 9 compares sedimentation- and DIA-derived PSDs for three $CaCO_3$ grades (F8 in Fig. 9a, F22 in Fig. 9b and F150 in Fig. 9c). For all grades, the sedimentation PSD lies closest to the DIA curves based on minimum-dimension size definitions, i.e., those yielding the smallest equivalent diameters.

For $CaCO_3$ F8 and $CaCO_3$ F22, the sedimentation PSD is in near agreement with the $x_{L,\mathrm{min}}$-based DIA PSD over the intermediate size range, but the curves progressively diverge towards the fine tail (approximately below 10 µm to 20 µm), with sedimentation shifting towards smaller equivalent diameters.

The F150 results further highlight the applicability limits of sedimentation-based sizing for coarser particles. In this case, the sedimentation test captures only the finer portion of the sample and does not reproduce the coarse end of the distribution, consistent with the commonly cited upper size limit for hydrometer/sedimentation methods (typically around 75 µm). Overall, Fig. 9 indicates that sedimentation and DIA can yield comparable PSDs when DIA is interpreted through minimum-dimension metrics, but that agreement decreases towards the finest sizes and can break down for samples with a substantial fraction above the sedimentation validity range.

Comparison between sedimentation- and DIA-derived PSDs for the natural fine materials is shown in Fig. 10. For barite (Fig. 10a), the sedimentation PSD falls within the DIA envelope and is closest to the lower-diameter DIA definitions (e.g., minimum-type metrics). Again, a progressive divergence was observed in the fine tail (around 10 µm and below), with sedimentation reporting a higher percentage of fines than DIA for a given diameter.

For the clay minerals (kaolinite and bentonite), substantially larger discrepancies were observed. In kaolinite (Fig. 10b), the sedimentation curve is markedly shifted towards smaller equivalent diameters relative to all DIA size definitions, indicating that sedimentation interprets the material as significantly finer. In bentonite (Fig. 10c),

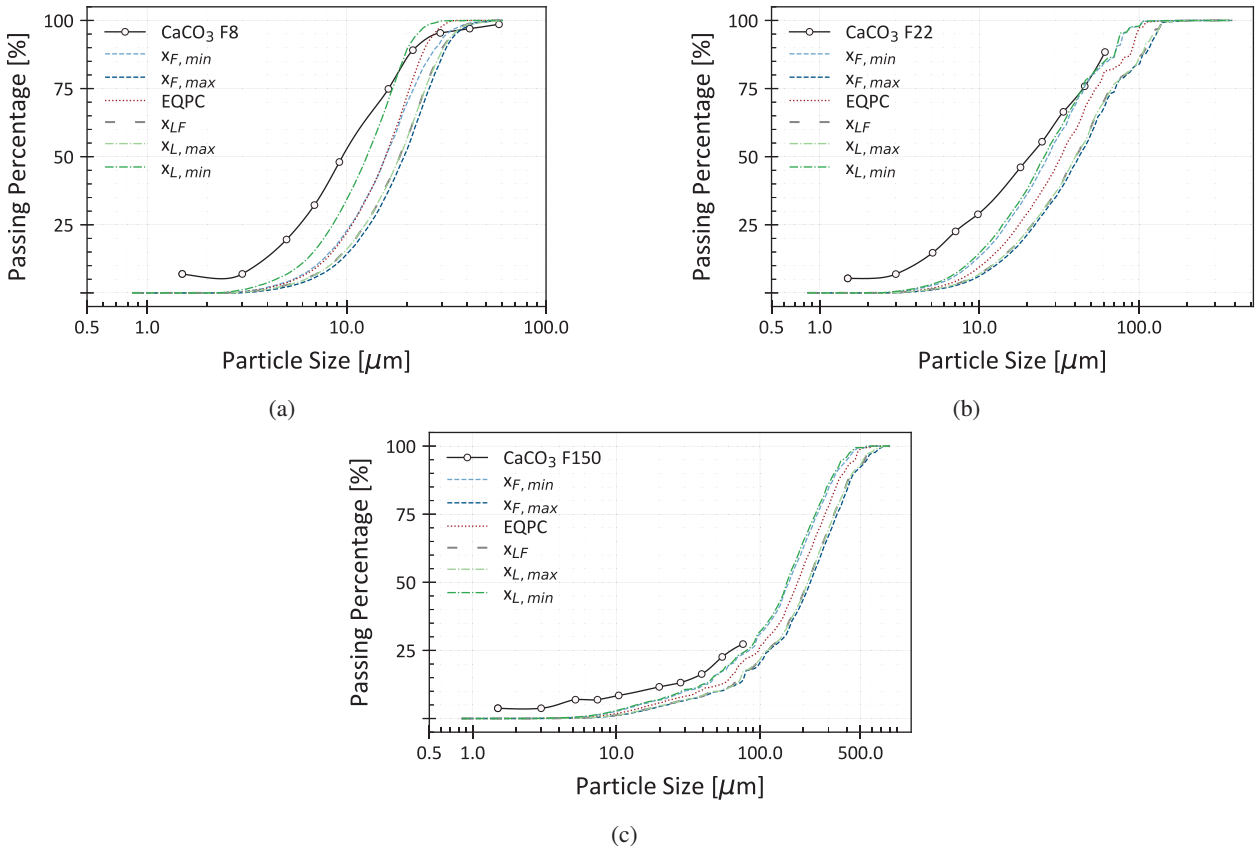

Figure 9: Comparison between PSDs obtained by sedimentation and by dynamic image analysis (DIA) for size-controlled reference materials: (a) $CaCO_3$ fraction F8; (b) $CaCO_3$ fraction F22; (c) $CaCO_3$ fraction F150.

sedimentation indicates a very large fine fraction already at the smallest reported sizes, whereas the DIA curves did not capture the same ultrafine component, resulting in a pronounced separation between the methods. These differences are consistent with the fact that, for platy particles, sedimentation-derived equivalent diameters are influenced by orientation-dependent drag during settling (Kuehn et al., 2024; Lu et al., 2000).

The DIA measurements for fines typically analysed on the order of 3×10^4 to 1×10^5 particles per sample using only a small amount of material. This high particle count supports representative PSD estimation while requiring substantially less specimen mass than conventional sedimentation tests, which typically involve sample masses of tens of grams, preparation of the full suspension, and test durations of up to 24 h; by contrast, DIA measurements are typically completed within a few minutes.

3.2. Dry sieving versus dynamic image analysis (QicPic)

3.2.1. QicPic data reduction and choice of bin number

To post-process the QicPic particle-level data, the PSD can be reconstructed either directly from the individual particles (reference) or by grouping particles into a user-defined number of size classes (bins), as implemented in the QicPic software. Because the choice of the number of classes, n, can influence derived grading descriptors, a bin-sensitivity analysis was performed to identify a practical and robust value of n for this study.

PSDs were reconstructed using $n = \{5, 10, 20, 50, 100\}$ classes (both linearly and logarithmically spaced). For each n, the uniformity coefficient $U = D_{60}/D_{10}$ and curvature coefficient $C_c = 2D_{30}/(D_{60}D_{10})$ were computed and compared to the particle-level reference. The results showed rapid convergence of both coefficients with increasing n: beyond $n = 20$, the differences became small, and $n = 50$ provided essentially converged values. For the relatively uniform sieve fractions, linear and logarithmic binning gave very similar results, as expected because each fraction spanned only about one order of magnitude in particle size. Linear spacing was therefore adopted for these materials.

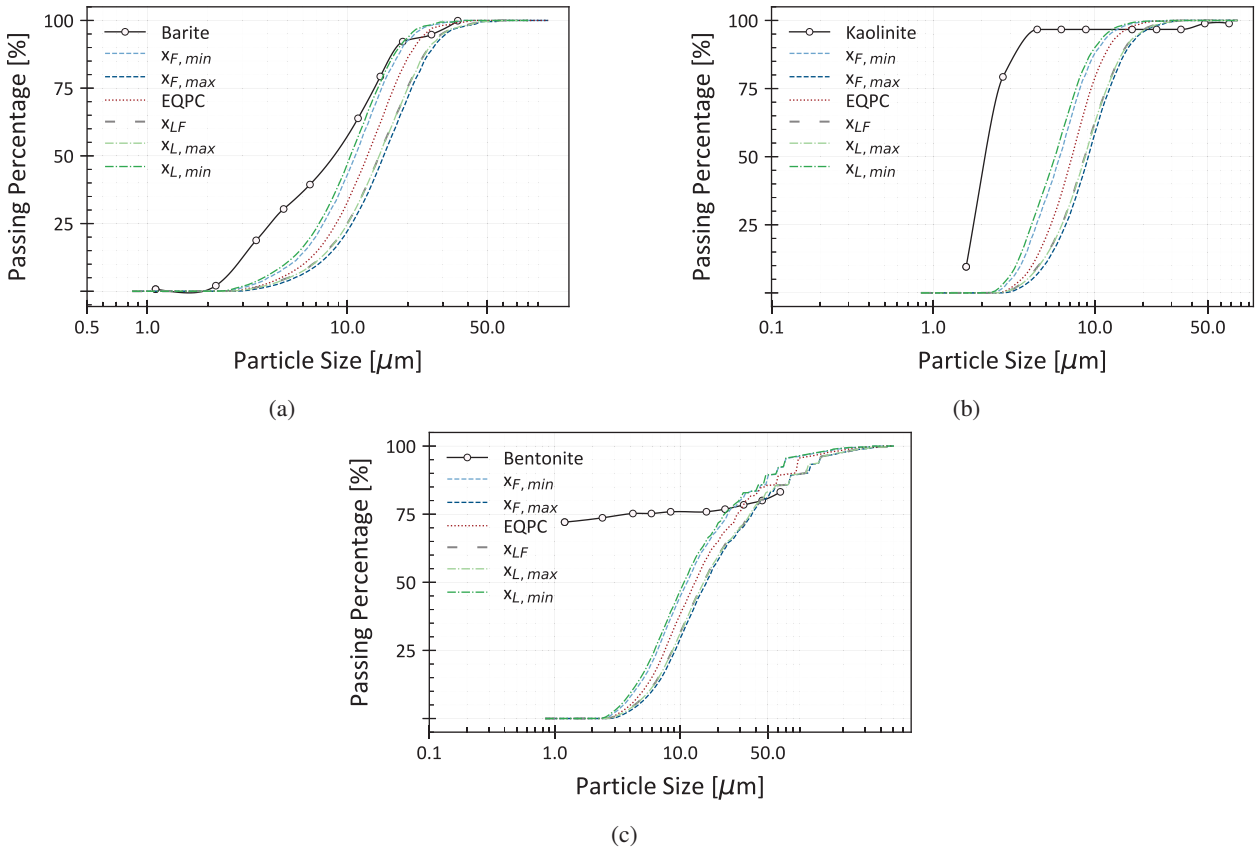

Figure 10: Comparison between sedimentation-derived PSDs and DIA-derived PSDs for natural fine materials: (a) barite, (b) kaolinite, and (c) bentonite.

By contrast, the non-uniform sharp sand covered a broader size range, and logarithmically spaced bin edges were used instead. In this case, linear bins tended to over-aggregate the fine fraction and under-resolve the lower end of the PSD, whereas log spacing provided better resolution at small sizes while still capturing the coarse tail consistently.

On this basis, $n = 50$ was adopted as a practical range for class-based PSD reconstruction, providing stable estimates of U and C_c while avoiding unnecessary over-resolution of the distribution (i.e., introducing noise due to a limited number of particles per class (Bishop and Nasrabadi, 2006; Olson, 2018)). Tab. 3 summarises this analysis for representative coarse materials (including risoni and tempestine as end-members in aspect ratio, and a sand sample), reporting the maximum relative deviations of U and C_c from the particle-level reference.

3.2.2. Manufactured shape-controlled coarse particles

Fig. 11 compares dry sieving and QicPic-derived PSDs for the shape-controlled coarse particles: risoni (Fig. 11a), puntine (Fig. 11b) and tempestine (Fig. 11c). Across all three pasta types, the QicPic PSD based on the minimum-dimension metric (MIC) provides the closest agreement with the sieve-based PSD. This indicates that, for these non-spherical particles, the sieve response is primarily governed by the controlling (smallest) particle dimension, consistent with the physical requirement for a particle to pass through an aperture.

For all samples, the alternative QicPic size definitions (EQPC, PED and MCC) yield systematically larger equivalent diameters than sieving. The separation between MIC and the larger-diameter metrics (particularly MCC) increased as particles became more elongated (i.e., as the aspect ratio decreased), whereas the more compact particles showed a smaller spread between the different equivalent-diameter definitions.

A further difference between the methods relates to discretisation. While the sieve PSD was constrained by the finite set of available sieve apertures, the QicPic particle-level data allowed the PSD to be reconstructed with a larger number of classes (here $n = 50$), providing a finer resolution of the distribution. This higher resolution improved the

Table 3
Sensitivity of grading coefficients to the number of bins n used to reconstruct PSDs from QicPic particle-level data. Values report the maximum relative deviation from the particle-level reference across the four equivalent diameters (EQPC, PED, MIC, MCC)

n	$\max(\lvert\Delta U\rvert/U)$ [%]	$\max\left(\lvert\Delta C_c\rvert/C_c\right)$ [%]
Risoni		
5	10.03	10.72
10	3.21	8.72
20	0.61	3.69
50	0.09	0.45
100	0.15	0.49
Tempestine		
5	9.22	12.35
10	2.60	3.36
20	0.73	1.53
50	0.12	0.35
100	0.15	0.15
Sand: LBS-B		
5	16.70	12.13
10	14.05	10.46
20	4.15	2.06
50	0.48	0.35
100	0.13	0.15

definition of the transition from complete passing to partial retention (i.e., the onset of the coarse tail) and yielded smoother PSD curves, which in turn supported more stable estimates of grading descriptors such as U and C_c.

Fig. 12 summarises the correlations between QicPic size and shape descriptors for the shape-controlled coarse particles: *risoni* (Fig. 12a), *puntine* (Fig. 12b) and *tempestine* (Fig. 12c). These three materials span a wide range of aspect ratios, from markedly elongated *risoni* ($AR \approx 0.32$) to the more compact *tempestine* ($AR \approx 0.73$), with *puntine* as an intermediate case ($AR \approx 0.50$).

A key outcome illustrated in Fig. 12 is that the minimum-dimension metric (MIC) exhibited the weakest correlations, particularly for the elongated particles. This was observed both in its correlations with the other size indices and, particularly, in its correlations with the shape descriptors. In practical terms, MIC appeared to carry the least information about projected particle shape, even though it provided the closest agreement with dry sieving (Fig. 11). This supports the interpretation that sieve-based sizing is primarily governed by a controlling (minimum) dimension and is not, by itself, a reliable indicator of overall particle morphology.

The overall correlation structure changes across the pasta types. Correlations were strongest for *risoni* and generally decrease moving towards the more compact *tempestine*, reflecting the reduced geometric contrast within the particle population as the aspect ratio approached unity. In addition, most size indices showed negative correlations with shape factors such as sphericity and roundness, indicating that particles classified as smaller by a given size definition tend to be associated with more circular projections. This trend was consistent with the measurement geometry of elongated particles: when a particle was captured in an orientation that yields a smaller projected size (e.g., aligned with its long axis), the corresponding 2D silhouette tends to appear less elongated and therefore more circular.

Among the size metrics, PED showed the strongest overall coupling with the shape descriptors, which was expected because perimeter-based measures are sensitive to particle elongation and boundary complexity (Maria and Carey, 2002). By contrast, convexity (or solidity) exhibits weak correlations with both size and other shape indices, largely because it remains close to unity for all pasta types, indicating limited variability in this descriptor across the tested particles.

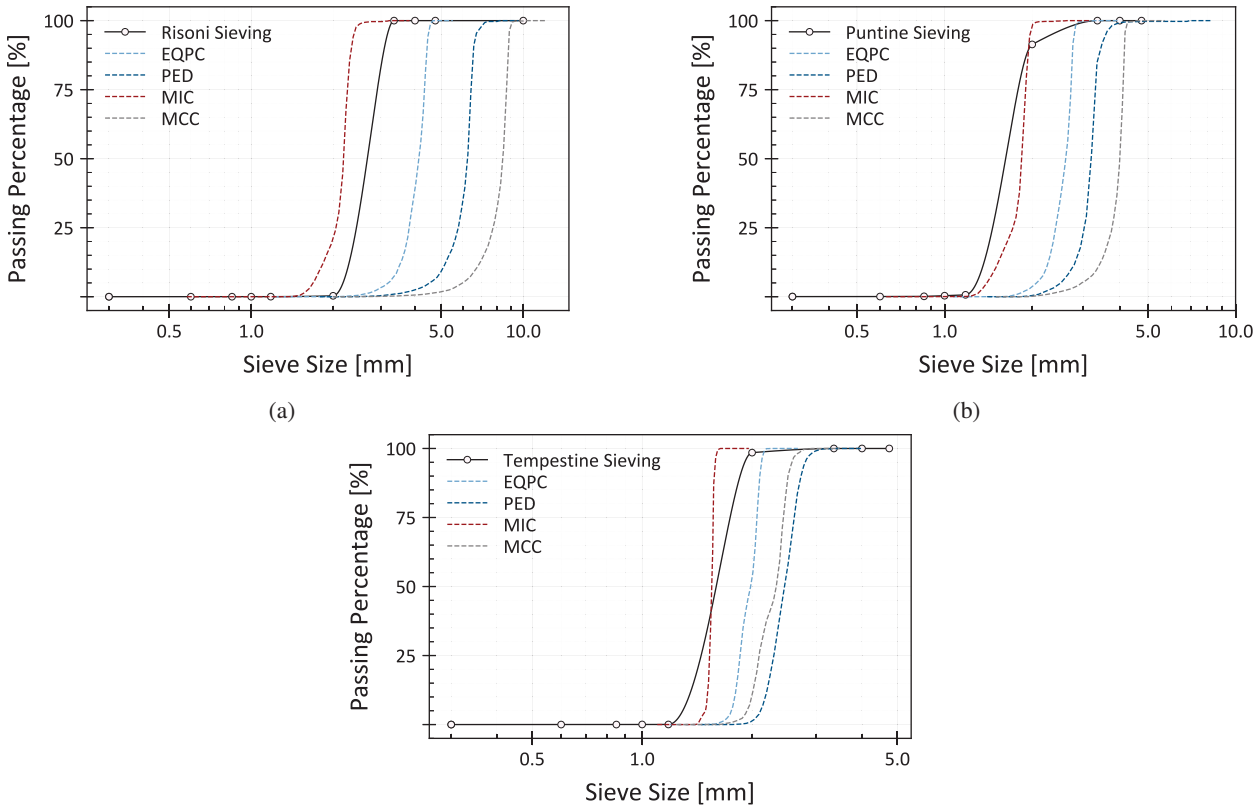

Figure 11: Comparison between dry sieving and QicPic-derived PSDs for the shape-controlled coarse particles: (a) risoni; (b) puntine; and (c) tempestine. QicPic PSDs are shown for the different equivalent diameter definitions (EQPC, PED, MIC and MCC), reconstructed using $n = 50$ classes.

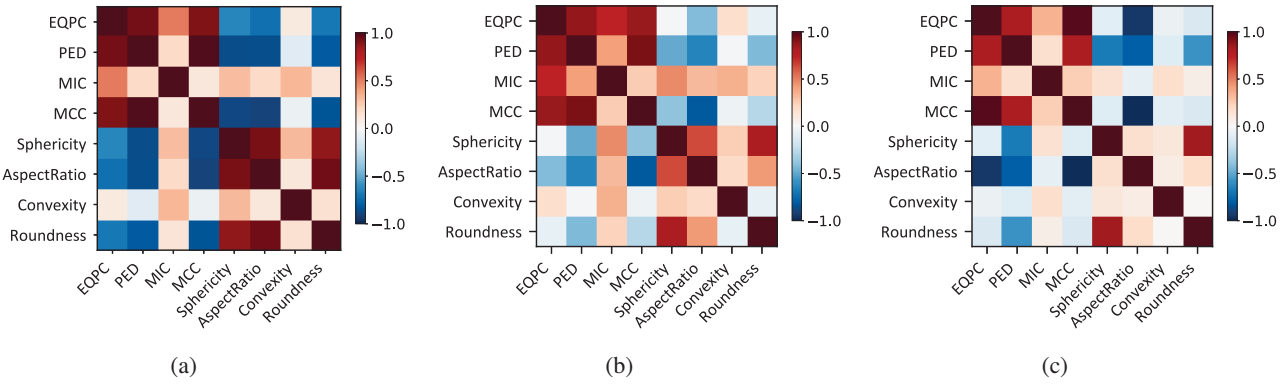

Figure 12: Correlation matrices between QicPic size and shape descriptors for the shape-controlled coarse particles: (a) risoni; (b) puntine; (c) tempestine.

3.3. Sieved quartz sand fractions

Fig. 13 compares the sieve-based PSDs with the PSDs reconstructed from QicPic for the sand fractions. Overall, the minimum-dimension metric (MIC) provided the closest agreement with the sieve results, whereas the alternative QicPic size definitions (EQPC, PED, and MCC) yield systematically larger equivalent diameters. This trend is consistent with the physical basis of sieving: passage through a mesh aperture is governed primarily by a particle's controlling

(minimum) dimension, while area-, perimeter- and circumscribed-circle based definitions reflect larger characteristic dimensions of the 2D projection.

A marked discrepancy between sieving and DIA was observed only for the non-uniform sharp sand, for which sieving did not capture the trend below 630 µm as clearly as DIA, see Fig. 13a. A likely explanation is that this material consisted of a dominant fine fraction together with a smaller coarse fraction; because a relatively large specimen mass (approximately 500 g, rather than 200 g) was required, the abundant fine fraction (greater than 300 g) likely promoted blinding of the 630 µm sieve. This suggests that, for strongly non-uniform sands, dry sieving may become less reliable when a large proportion of the material accumulates on a single sieve.

Compared with the pasta datasets, the spread between the different QicPic size definitions was smaller for the sand fractions, reflecting their more equant morphology and the narrower range of aspect ratios. Nevertheless, Fig. 13 shows that the choice of equivalent diameter remains important when interpreting DIA-derived PSDs, even for granular sands, and should be stated explicitly when comparing to conventional sieve results.

The QicPic results were also obtained from comparatively small sample masses. For the coarse materials, each measurement typically analysed 3×10^3 to 7×10^3 particles, corresponding to approximately 10 g to 20 g of material (about 3–5 teaspoons). Despite this limited mass, the QicPic-derived PSDs reproduce the key features of the sieve-based distributions (Fig. 13), indicating that a few thousand particles are sufficient to obtain a representative grading for these sands. By comparison, standard sieve analyses for the sand fractions considered here typically require substantially larger specimen masses (on the order of 50 g to 200 g), depending on the applicable standard and maximum particle size (Head, 1992). Therefore, DIA can provide comparable PSD information with a markedly reduced material and time requirement.

Fig. 14 shows example correlation matrices between QicPic size indices and shape descriptors for two Leighton Buzzard sand fractions: Fraction B (Fig. 14a) and Fraction E (Fig. 14b). These two fractions were selected because they showed contrasting behaviour and together are representative of the range observed across the sand dataset.

For both fractions, the different QicPic size indices were strongly and positively correlated with each other, indicating that they track a common underlying size signal within each fraction (top-left blocks of the correlation matrix). However, MIC consistently exhibits the weakest correlation with the other size indices, particularly with MCC (and to a lesser extent with PED), and this effect was more pronounced in Fraction E. This again reflects that MIC captures a controlling/minimum dimension that can vary somewhat independently of the larger characteristic dimensions represented by MCC and perimeter-based measures.

The coupling between size and shape descriptors differs between the two fractions. Fraction B showed a comparatively clear and internally consistent correlation pattern: the shape descriptors were reasonably correlated with each other (bottom-right block), and the correlations between size indices and shape descriptors indicated systematic within-sample trends, such as a positive correlation between size and sphericity and negative correlations between size and convexity and roundness. Interpreted physically, this indicates that within Fraction B larger particles tend to be more isotropic in shape in projection, while the smallest particles tend to be more convex/rounded, consistent with a size-dependent morphology within the same nominal fraction.

By contrast, Fraction E exhibits weaker and more mixed size–shape correlations, indicating a less systematic coupling between particle size and the selected shape descriptors. In particular, MIC and MCC can show opposing correlations with aspect ratio (MIC positive, MCC negative), highlighting that different equivalent diameter definitions can emphasise different geometric dimensions of the same particle population. Overall, these matrices illustrate that a single shape index is generally insufficient to characterise the morphology of a granular fraction; rather, the combined set of descriptors is needed to identify (or exclude) size-dependent morphology trends. A more detailed examination of these patterns is left for future work, as it goes beyond the main scope of the present method-comparison study.

4. Conclusions

This study assessed whether conventional PSD methods (dry sieving and sedimentation) remain fit for purpose when compared with dynamic image analysis (DIA), using both manufactured reference particles with controlled geometry and engineering materials commonly encountered in research and practice. The main findings can be summarised as follows:

- DIA-derived PSDs depended strongly on the selected equivalent diameter. For a given material, different DIA size definitions produced different PSDs, and the spread increased with particle elongation.

- For coarse particles, dry sieving was governed primarily by a controlling (minimum) dimension. For both the shape-controlled pasta particles and the quartz sand fractions, the QicPic minimum-dimension metric (MIC) showed the closest agreement with sieve-based PSDs, whereas EQPC, PED and MCC systematically returned larger equivalent diameters. This supports the interpretation of sieve size as an orientation-dependent, aperture-controlled measure rather than a unique geometric diameter.

- The non-uniform *sharp sand* highlighted a practical limitation of dry sieving. In this broad bimodal material, the sieve-based PSD did not capture the grading trend in the fine tail as clearly as QicPic, likely because the relatively large specimen mass required for the coarse fraction promoted accumulation and possible blinding during sieving. This suggests that, for sands spanning a wide size range, conventional sieving may become less reliable unless the sieving strategy is adapted, whereas DIA can reproduce the continuous PSD more robustly in such cases.

- For fine particles, sedimentation generally aligned best with minimum-dimension DIA metrics, but agreement decreased in the finest range. For cellulose and for $CaCO_3$ grades within the sedimentation domain, sedimentation PSDs were closest to minimum-type DIA definitions and diverged progressively towards smaller sizes (approximately below 10 µm to 20 µm), with sedimentation shifting to smaller equivalent diameters.

- The applicability limits of sedimentation were evident for coarser fines. For $CaCO_3$ F150, sedimentation captured only the fine portion of the sample and did not reproduce the coarse end of the PSD, consistent with the commonly cited upper validity limit for hydrometer/sedimentation methods (around 75 µm).

- Clay-rich materials showed the largest discrepancies between methods. Kaolinite and bentonite exhibited the greatest differences between sedimentation- and DIA-derived PSDs, indicating that, for platy or anisotropic particles, shape-related settling effects and suspension conditions can strongly influence the comparison and must be considered when interpreting sedimentation-based equivalent diameters.

- QicPic class definition could be selected efficiently without loss of accuracy. The bin-sensitivity analysis showed rapid convergence of grading descriptors with increasing number of classes; selecting $n \approx 20$ to 50 bins was sufficient to stabilise U and C_c while avoiding over-resolution caused by a limited number of particles per class.

- DIA reduced specimen-mass requirements while maintaining representative PSD estimates. For the coarse materials, a few thousand analysed particles were sufficient to reproduce the main features of the sieve-based PSDs, which are typically obtained from substantially larger specimen masses. At the same time, the smaller sample mass used in DIA means that greater care is required to ensure that the analysed subsample is representative of the bulk material. For the fine materials, DIA routinely analysed 3×10^4 to 1×10^5 particles per sample using only small amounts of material.

Overall, the results indicate that conventional methods remain acceptable as reference procedures in many routine cases, such as equant sands and fines within the validity range of sedimentation. However, they should be interpreted as *method-defined* size measures whose bias increases for anisotropic particles and clay-rich suspensions. DIA provides a complementary route that can reproduce conventional PSDs when an appropriate equivalent diameter is selected, while also providing morphology information that is inaccessible to sieving and sedimentation. These findings support improved reporting practice, and potentially future updates to standards, by requiring explicit statement of the DIA size definition used and by clarifying how equivalent spherical diameters from sedimentation should be interpreted for non-spherical particles.

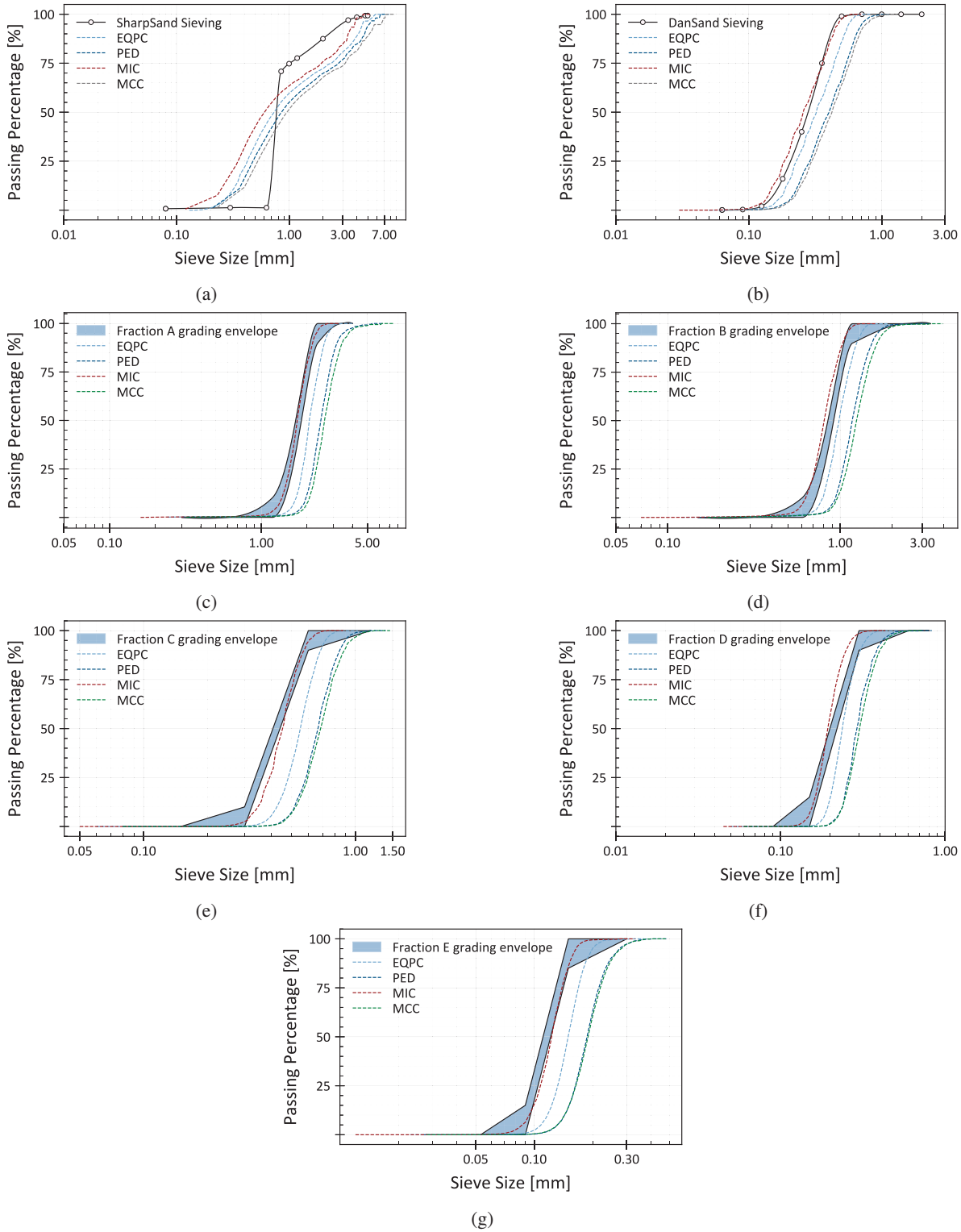

Figure 13: Comparison between sieve-based PSDs and QicPic-derived PSDs for the sand materials analysed: (a) Sharp Sand; (b) Danish sand and (c–g) Leighton Buzzard sand fractions A–E. QicPic PSDs are reconstructed using $n = 50$ classes.

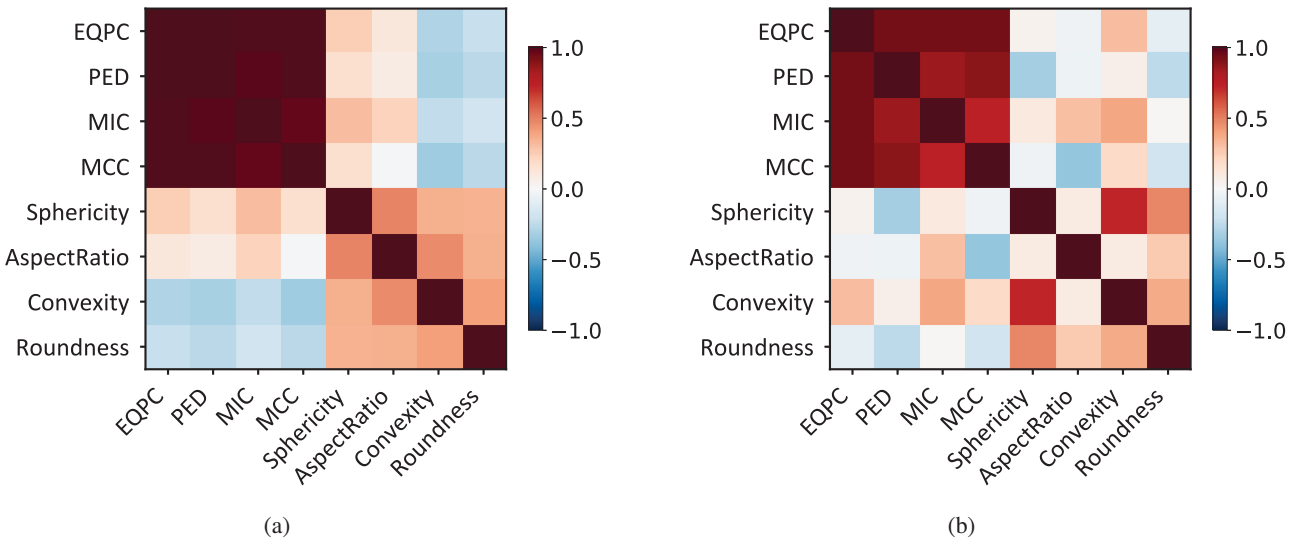

Figure 14: Correlation matrices between QicPic size indices and shape descriptors for two Leighton Buzzard sand fractions: (a) Fraction B; (b) Fraction E.

Nomenclature

AR	Aspect ratio
C_c	$= \frac{D_{30}^2}{D_{60} \cdot D_{10}}$ Coefficient of curvature
C_v	Convexity
D_i	representative particle diameter of size class i [L]
DIA	Dynamic image analysis
$EQPC$	Area-equivalent diameter [L]
MCC	Minimum circumscribed circle diameter [L]
MIC	Maximum inscribed circle diameter [L]
n	Number of classes
PED	Perimeter-equivalent diameter [L]
PSD	Particle Size Distribution
R	Roundness
S	Sphericity
U	$= D_{60}/D_{10}$ Coefficient of uniformity
$x_{F,max}$	Maximum Feret diameter [L]
$x_{F,min}$	Minimum Feret diameter [L]
x_{LF}	Length-based diameter [L]
$x_{L,max}$	Maximum length-based diameter [L]
$x_{L,min}$	Minimum length-based diameter [L]

Diameter values are presented in mm for coarse materials and in µm for fine materials.

Acknowledgements

GS would like to express his sincere appreciation to Prof. Giulia Viggiani for introducing him to the topic of particle-shape investigation and for inspiring the use of pasta as a manufactured reference material with reproducible geometry.

Funding

This research received no external funding.

Data Availability Statement

Data are available from the corresponding authors upon reasonable request.

CRediT authorship contribution statement

Gianmario Sorrentino: Conceptualization, Data curation, Formal analysis, Investigation, Methodology, Validation, Software, Visualization, Writing – original draft. **Mauro Muñiz-Menéndez:** Formal analysis, Investigation, Conceptualization, Writing & Editing.. **Pieter Desnerck:** Formal analysis, Investigation, Writing & Editing..

References

Al-Hashemi, H. M. B., Al-Amoudi, O. S. B., Yamani, Z. H., Mustafa, Y. M., and Ahmed, H.-u.-R. (2021). The validity of laser diffraction system to reproduce hydrometer results for grain size analysis in geotechnical applications. *PloS one*, 16(1):e0245452.

Allen, T. (1990). Sieving. In *Particle Size Measurement*, pages 192–216. Springer.

ASTM, C. D.-. (2009). *Standard test methods for particle-size distribution (gradation) of soils using sieve analysis*. ASTM International.

ASTM International (2000). Standard test methods for amount of material in soils finer than the no. 200 (75-μm) sieve. ASTM D1140.

ASTM International (2004). Standard test methods for particle-size distribution (gradation) of soils using sieve analysis. ASTM D6913-04.

ASTM International (2021). Standard specification for woven wire test sieve cloth and test sieves. ASTM E11.

Bareither, C. A., Edil, T. B., Benson, C. H., and Mickelson, D. M. (2008). Geological and physical factors affecting the friction angle of compacted sands. *Journal of geotechnical and geoenvironmental engineering*, 134(10):1476–1489.

Barnes, G. (2017). *Soil mechanics*. Bloomsbury Publishing.

Bartley III, P. C., Jackson, B. E., and Fonteno, W. C. (2019). Effect of particle length to width ratio on sieving accuracy and precision. *Powder Technology*, 355:349–354.

Bishop, C. M. and Nasrabadi, N. M. (2006). *Pattern recognition and machine learning*, volume 4. Springer.

Bittelli, M., Pellegrini, S., Olmi, R., Andrenelli, M. C., Simonetti, G., Borrelli, E., and Morari, F. (2022). Experimental evidence of laser diffraction accuracy for particle size analysis. *Geoderma*, 409:115627.

British Standards Institution (2020). Tests for geometrical properties of aggregates — part 2: Determination of particle size distribution — test sieves, nominal size of apertures. BS EN 933-2:2020.

Callesen, I., Palviainen, M., Armolaitis, K., Rasmussen, C., and Kjønaas, O. J. (2023). Soil texture analysis by laser diffraction and sedimentation and sieving–method and instrument comparison with a focus on nordic and baltic forest soils. *Frontiers in Forests and Global Change*, 6:1144845.

Cavallaro, A., Maugeri, M., and Mazzarella, R. (2001). Static and dynamic properties of leighton buzzard sand from laboratory tests.

Cho, G.-C., Dodds, J., and Santamarina, J. C. (2006). Particle shape effects on packing density, stiffness, and strength: natural and crushed sands. *Journal of geotechnical and geoenvironmental engineering*, 132(5):591–602.

Eshel, G., Levy, G. J., Mingelgrin, U., and Singer, M. J. (2004). Critical evaluation of the use of laser diffraction for particle-size distribution analysis. *Soil Science Society of America Journal*, 68(3):736–743.

Falahati, N., Routh, A. F., and Chellappah, K. (2020). The effect of particle properties and solids concentration on the yield stress behaviour of drilling fluid filter cakes. *Chemical Engineering Science: X*, 7:100062.

Fernlund, J. M. (1998). The effect of particle form on sieve analysis: a test by image analysis. *Engineering Geology*, 50(1-2):111–124.

Forsdyke, J. C. and Lees, J. M. (2025). Influence of crack width on carbonation depths in functionally layered concrete. *Materials and Structures*, 58(4):130.

Germaine, J. T. and Germaine, A. V. (2009). *Geotechnical laboratory measurements for engineers*. John Wiley & Sons.

Head, K. H. (1992). *Manual of soil laboratory testing. Volume 1. Soil classification and compaction tests*.

International Organization for Standardization (1990). Test sieves — metal wire cloth, perforated metal plate and electroformed sheet — nominal sizes of openings. ISO 565:1990.

International Organization for Standardization (2016). Part 4: Determination of particle size distribution. ISO 17892-4:2016.

International Organization for Standardization (2020). Particle size analysis — laser diffraction methods. ISO 13320:2020.

International Organization for Standardization (2021). Particle size analysis — image analysis methods — part 2: Dynamic image analysis methods. ISO 13322-2:2021.

Jayaweera, K. and Mason, B. (1965). The behaviour of freely falling cylinders and cones in a viscous fluid. *Journal of Fluid Mechanics*, 22(4):709–720.

Jeffery, G. B. (1922). The motion of ellipsoidal particles immersed in a viscous fluid. *Proceedings of the Royal Society of London. Series A, Containing papers of a mathematical and physical character*, 102(715):161–179.

Kenney, T. (1967). The influence of mineral composition on the residual strength of natural soils.

Krumbein, W. C. and Sloss, L. L. (1963). *Stratigraphy and sedimentation*, volume 71. LWW.

Kuehn, R., Kilian, R., Lang, D., Morales, L. G., Grendal, O. G., and Stipp, M. (2024). Clay alignment takes place during early stages of sedimentation. *Communications Earth & Environment*, 5(1):696.

Li, L. and Iskander, M. (2020). Evaluation of dynamic image analysis for characterizing granular soils. *Geotechnical Testing Journal*, 43(5):1149–1173.

Lopez, A., Gustavsson, H., and Korkiala-Tanttu, L. (2021). Comparison between hydrometer and laser diffraction methods in the determination of clay content in fine-grained soils. In *IOP Conference Series: Earth and Environmental Science*, volume 710, page 012012. IOP Publishing.

Lu, N., Ristow, G. H., and Likos, W. J. (2000). The accuracy of hydrometer analysis for fine-grained clay particles. *Geotechnical Testing Journal*, 23(4):487–495.

Maria, A. and Carey, S. (2002). Using fractal analysis to quantitatively characterize the shapes of volcanic particles. *Journal of Geophysical Research: Solid Earth*, 107(B11):ECV–7.

McNown, J. S. and Malaika, J. (1950). Effects of particle shape on settling velocity at low reynolds numbers. *Eos, Transactions American Geophysical Union*, 31(1):74–82.

Michaelides, E. E. (2026). The equation of motion of particles in fluids—an historical perspective. *Powders*, 5(1):5.

Mitchell, J. and Soga, K. (2005). Fundamentals of soil behavior.

Nasser, M. and James, A. (2006). Settling and sediment bed behaviour of kaolinite in aqueous media. *Separation and Purification Technology*, 51(1):10–17.

Olson, E. (2018). A study of the effects of histogram binning on the accu-racy and precision of particle sizing measurements. *Pharm Technol*, 42:28–33.

Otim, G. I., Zhelezova, A., Sorrentino, G., Trapp, S., and Rocchi, I. (2025). Hydraulic properties of rooted soils from salix sp. pot experiments. In *E3S Web of Conferences*, volume 642, page 06009. EDP Sciences.

Penna, A., Sorrentino, G., d'Onofrio, A., Silvestri, F., Simonelli, A. L., et al. (2016). Dynamic behaviour of the leighton buzzard sand-b under very low confining stresses. In *Proceedings of the 1st IMEKO TC4 International Workshop on Metrology for Geotechnics (MetroGeotechnics 2016), Benevento, Italy*, pages 17–18.

Pons, M.-N. and Dodds, J. (2015). Particle shape characterization by image analysis. In *Progress in filtration and separation*, pages 609–636. Elsevier.

Powers, M. C. (1953). A new roundness scale for sedimentary particles. *Journal of Sedimentary Research*, 23(2):117–119.

Rabinski, G. and Thomas, D. (2004). Dynamic digital image analysis: emerging technology for particle characterization. *Water Science and Technology*, 50(12):19–26.

Ranville, J. and Montano, M. D. (2015). Size distributions. In *Frontiers of Nanoscience*, volume 8, pages 91–121. Elsevier.

Ryzak, M. and Bieganowski, A. (2010). Determination of particle size distrubution of soil using laser diffraction-comparison with areometric method. *International Agrophysics*, 24(2):177–181.

Sedláčková, K., Ševelová, L., Igaz, D., and Aydın, E. (2024). Determination of particle size distribution: comparison of standard hydrometer method and laser diffraction analysis for use in forestry. *Forests*, 15(2):327.

Senetakis, K., Coop, M. R., and Todisco, M. C. (2013). The inter-particle coefficient of friction at the contacts of leighton buzzard sand quartz minerals. *Soils and Foundations*, 53(5):746–755.

Sheikh, M. Z., Gustavsson, K., Lopez, D., Lévêque, E., Mehlig, B., Pumir, A., and Naso, A. (2020). Importance of fluid inertia for the orientation of spheroids settling in turbulent flow. *Journal of Fluid Mechanics*, 886:A9.

Sorrentino, G. (2022). *Effects of filtration process variables on filter cake properties and formation*. PhD thesis.

Sorrentino, G. and Biscontin, G. (2023). Improved filtration parameters from modified api filter press. *Geoenergy Science and Engineering*, 224:211605.

Sorrentino, G. and Franza, A. (2025). Experimental study of sugar-induced sand cementation in dry conditions. *Geomechanics for Energy and the Environment*, page 100765.

Sorrentino, G., Gajjar, P., Chellappah, K., Biscontin, G., and Withers, P. J. (2025). Filter cake formation and particle invasion: A comparative study of obm and wbm in wellbore applications. *Powder Technology*, page 121777.

Urciuoli, G. (2007). Lecture slides on sieving-based particle-size measurement. Course lecture material, *Geotecnica*, Università degli Studi di Napoli Federico II. Figure adapted from lecture slides.

Wang, X., Tian, K., Su, D., and Zhao, J. (2019). Superellipsoid-based study on reproducing 3d particle geometry from 2d projections. *Computers and Geotechnics*, 114:103131.

Weiss, P., Erickson, A., Hettler, E., and Gulliver, J. (2013). The importance of particle size distribution on the performance of sedimentation practices. *Optimizing stormwater treatment practices: a handbook of assessment and maintenance. Springer, New York*.

Yokojima, S., Takashima, R., Asada, H., and Miyahara, T. (2021). Impacts of particle shape on sedimentation of particles. *European Journal of Mechanics-B/Fluids*, 89:323–331.

Zheng, J. and Hryciw, R. D. (2016). Index void ratios of sands from their intrinsic properties. *Journal of Geotechnical and Geoenvironmental Engineering*, 142(12):06016019.